1   **Passive carbon sequestration associated with wollastonite mining, Adirondack Mountains,**

2   **New York**

3

4   **Revision 1**

5

6   Word Count: 5252

7

8   William H. Peck, Dianne Keller, Victoria S. Arnold, Faith McDonald, Lily C. Kuentz, and Paul

9   M. Nugent

10   Department of Geology, Colgate University, Hamilton NY 13346

11

12   **Abstract**

13   Crushed ore in Adirondack wollastonite mines (New York) shows textural evidence for

14   wollastonite dissolution and cementation by calcite and opal. The reaction $CaSiO_3 + CO_2 =$

15     $CaCO_3 + SiO_2$ is a model reaction for silicate weathering and carbonation that has not been

16   characterized in the field until now (outside of controlled experiments). Cemented samples from

17   the Lewis and Fox Knoll mines contain up to 3% and 6% calcite respectively, and contain

18   modern [14]C. Carbon isotope ratios have an organic signature at both mines but more strongly at

19   Lewis (δ^{13}C from -9‰ to -29‰ VPDB) which, along with observed filamentous biofilms,

20   supports a microbial role in mineralization.

21   Differences are seen between wollastonite weathering in these mines versus wollastonite

22   weathering in lab experiments and field studies of carbonate formation in other rock types.

23   Grains surrounded by reaction products reach complete dissolution here, indicating that

24   passivation by jacketing is not important at the field sites. Also, dissolved ions do not all form in-

25   situ reaction products, suggesting that solutes are leaving the system. A key finding of this study

26   is the strong organic $\delta^{13}C$ signature of calcite cements at the Lewis mine, which also show higher

27   calcite content per years of exposure compared to cements at the Fox Knoll mine. Although

28   microbial fractionation complicates isotopic assessment of atmospheric CO_2 sequestration, our

29   findings suggest sequestration rates are enhanced by geomicrobiological activity.

30

31   Keywords: Wollastonite weathering, Silicate carbonation, Carbon sequestration, Carbon

32   isotopes, Geomicrobiology, Acid precipitation

33

34   **Introduction**

35   Silicate weathering and the subsequent formation of carbonate minerals has long been

36   known to have a first-order control on Earth's carbon cycle (Urey, 1952), and more recently

37   weathering reactions have been looked to as a method for engineered carbon sequestration

38   (Oelkers and Cole, 2008). For the carbonate-silicate geochemical cycle, silicate weathering is

39   often described by using the simplified "Urey reaction" for wollastonite weathering and

40   carbonation, as a proxy for all silicates:

41   wollastonite + carbon dioxide = calcite + quartz. (1)

42                     $CaSiO_3 + CO_2 = CaCO_3 + SiO_2$
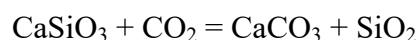
43   Wollastonite dissolution and carbonation has been investigated in the laboratory (e.g.,

44   Huijgen et al., 2006; Daval et al., 2009a,b; Schott et al., 2012; Di Lorenzo et al., 2018), and in

45   field studies on wollastonite 'liming' of watersheds and in agriculture (Shao et al., 2015; Haque

46   et al., 2020). Although this reaction is reported in the metamorphic petrology literature,

47   wollastonite weathering and carbonation in the field (outside of controlled experiments) has not

48   previously been characterized.

49   During research on wollastonite deposits in the Adirondack region of New York

50   (Barcello et al., 2018), we observed crusts of calcite-cemented crushed ore at the Lewis and Fox

51   Knoll mines, often having the aspect of concrete, and surmised that they formed via wollastonite

52   weathering according to the above reaction. Crushing enhances reaction rates and therefore, the

53   potential for C capture, which may help offset CO_2 emissions from mines (Power et al., 2013).

54   Here we show that microbially-mediated wollastonite dissolution and formation of opal and

55   calcite from atmospheric CO_2 is well developed in these, and likely other wollastonite mines. For

56   example, we also observe similar cemented mine wastes at the currently-operating Oak Hill mine

57   2.5 km east of Lewis, and the Valentine wollastonite mine in northwestern New York (Kasten et

58   al., 2022). Our results give new insights on approaches for C sequestration and the value of

59   using isotopes to enhance our understanding mineral weathering processes in natural systems.

60

61   **Geologic Setting**

62   Wollastonite ore in the Willsboro-Lewis wollastonite district occurs as coarse

63   wollastonite-garnet-pyroxene skarns found along the contact between anorthosite and country

64   rocks in the Adirondack Highlands (Whitney and Olmsted, 1998). The skarns and anorthosite are

65   thought to have formed 1155 Ma. Both were deformed and recrystallized at high grade 1090–

66   1020 Ma (Seman et al., 2017; Peck et al., 2018b) and show low $\delta^{18}O$ indicative of meteoric

67   water metasomatism (Valley and O'Neil, 1981; Barcello et al., 2018).

68   The mines in this district have accounted for the majority of US wollastonite production

69   throughout the history of the industry (Robinson et al., 2006; Peck and Bailey, 2008). If the

70 existing reserve were used for carbon sequestration, these deposits represent a storage potential

71 of 2-5 Mt of CO_2 (Lackner et al., 2012). Mining at Fox Knoll (near Willsboro) began as an open

72 pit, first intermittently from 1938–1953 and then consistently until 1960, when it moved

73 underground until 1982. The Lewis open-pit mine operated from 1980 until 2016, when

74 operations moved to Oak Hill. Although active mining has ended at both Lewis and Fox Knoll,

75 site maintenance is ongoing at both sites, and is more active at Lewis. The period of mining here

76 encompasses the peak of anthropogenic acid precipitation in northeastern America in the early

77 1970s and 1980s (often with pH <4), through a return to more natural pH levels due to US Clean

78 Air legislation in the 1990s (Likens et al., 2021). The Willsboro-Lewis region has a warm-

79 summer humid continental climate, with mean rainfall between 3.0 and 11.4 cm/month and

80 average temperatures ranging between -6.3 and 21.3°C (ncei.noaa.gov).

81

82   **Methods and Results**

83   The two mines investigated show different amounts and styles of wollastonite weathering

84 and cementation. At Lewis, cemented crushed ore is mainly observed as 2–20 cm thick, hard

85 slabs in berms and on roadways, and berm-capping crusts around the ore stockpile and

86 maintenance building parking area (Figs. 1A+B). Cementation of crushed ore is more extensive

87 at Fox Knoll, with cemented berm caps up to 30 cm thick, consisting of a crusted mixture of

88 crushed ore with some clasts of Proterozoic bedrock (Fig. 1C). In addition, distinct irregular

89 cemented lumps of aggregate are present on the Fox Knoll quarry floor (Fig. 1D). 1–1.5 m deep

90 pits dug into berms at both sites showed that the bulk of the ore stockpile material is loose and

91 predominantly uncemented, although cm-scale cemented nodules are observed.

92   Quantitative mineralogy, reported as weight %, was determined by RockJock analysis of

93   X-ray diffraction (XRD) patterns after Eberl (2003) (See Supplementary Materials[1]). Except for

94   one sample with 18% wollastonite, uncemented ore stockpile samples at Lewis contain 29–51%

95   wollastonite (Table 1), significantly more than cemented samples, which range from 7–21%.

96   Cemented ore calcite (0.7–2.8%) and opal (0.2–0.7%) contents at Lewis are higher than in

97   uncemented ore, where they are present in only trace amounts (both average ≤0.5%).

98   Uncemented ore at Fox Knoll has 23–43% wollastonite, 1.6–1.9% calcite, and 0.1–0.4% opal

99   (Table 1). As at Lewis, Fox Knoll cemented ore contains more calcite (1.8–6.1%) and opal (0.3–

100   1.7%) than uncemented samples. Calcite and opal contents in cemented Fox Knoll samples are

101   highly correlated to each other (r^2=0.96, n=6), and show a weak negative correlation to

102   wollastonite content (r^2=0.60 for calcite and 0.66 for opal). Plotted together, calcite and opal

103   contents for all samples from both sites also show a strong positive correlation (r^2=0.82, n=36;

104   Fig. 3).

105   Crushed ore at both sites consists mostly of sub-cm-sized angular clasts of wollastonite,

106   garnet, and pyroxene mixed with finer gravel through mud-size materials. Calcite and opal

107   precipitates coat mineral fragments and spread into pore spaces in cemented samples (Figs.

108   2A+B). Wollastonite commonly shows textural evidence for dissolution, partially controlled by

109   cleavage, leaving behind ribcage-like precipitated opal and/or calcite stockworks (Figs. 2B+C).

110   Pore spaces are decorated by ridged skins and lepidospheres (ie. spherical aggregates) of opal

111   and calcite precipitates (Fig. 2D), and a euhedral platy phase not detected by XRD (Figs. 2D+E).

112   Preliminary Raman spectroscopy indicates this platy phase may be the biomineral brushite.

113   Alternatively, an additional calcium hydroxide or calcium oxalate may be present. In many

114   samples, fixed with glutaraldehyde for imaging, minerals are coated with what appear to be

115   biofilms with associated filamentous material (Fig. 2F). Calcium-silicate-hydrate (CSH) gel

116   alteration products that have been described in carbonation of other calc-silicate minerals (e.g.

117   Milodowski et al., 2011), were not observed.

118   Stable isotopes of calcite were measured using dual-inlet gas mass spectrometry, and

119   accelerator mass spectrometry provided ^{14}C contents for select samples. Oxygen isotope ratios

120   for both mines span from 15.3 to 23.8‰ VSMOW, and do not correlate with δ^{13}C or mineralogy.

121   Carbon isotopes vary by deposit, ranging from -6.3 to -11.7‰ at Fox Knoll and -9.3 to -29.5‰

122   VPDB at Lewis (Fig. 3). Fox Knoll δ^{13}C values are relatively homogenous ($1\sigma=\pm1.4$‰), and do

123   not correlate with mineralogy. At Lewis, δ^{13}C correlates with calcite and opal content, and

124   samples with the lowest δ^{13}C have the most modern C (F^{14}C).

125

126   **Discussion**

127   **Evidence From Mineralogy and Textures**

128   Wollastonite dissolution in crushed ores from Lewis is most strongly evident in the

129   cemented samples, which average 12 wt. % less wollastonite than uncemented samples.

130   However, this trend is not seen for Fox Knoll. For both sites, wollastonite contents vary widely

131   in uncemented samples but are more consistent in cemented samples, which average 17.7±5.8%

132   (1σ) at Lewis and 39.2±5.1% at Fox Knoll. These averages represent losses of 65% and 40%

133   respectively, relative to average wollastonite contents of the original ore bodies, ($\approx$50% at Lewis,

134    $\approx$65% at Fox Knoll; Fig. 3A). Less calcite and opal are present than is predicted from this

135   amount of wollastonite dissolution (Fig. 3A), but the strong correlation of calcite and opal

136   contents along with their observed textural associations with wollastonite support that they

137   formed via reaction (1). The ca. 20–25% calcite 'missing' from stoichiometric wollastonite

138   weathering presumably left the system as aqueous Ca^{2+} and HCO_3^- to potentially precipitate as

139   soil carbonates, be biomineralized by terrestrial and freshwater biota, or eventually form marine

140   carbonate.

141   On average, cemented samples from both Fox Knoll and Lewis contain more calcite

142   (3.4% at Fox Knoll; 1.5% at Lewis) than opal (0.7% at Fox Knoll; 0.4% at Lewis). Although our

143   study did not include solution chemistry, calcite's greater abundance over opal in these samples

144   suggests more Si is leaving the system than Ca. This mineralogic finding parallels Ca and Si

145   fluxes observed in forested watersheds limed with wollastonite, where 11 years after liming,

146   4.8% of the Ca and 17% of the Si had left the watershed (Shao et al., 2015). Mean Ca:Si ratios

147   from that study of 0.1–0.3 for soil solutions and 0.3 in stream water coincide with the

148   opal:calcite ratio of 0.1 for uncemented samples and 0.3 for crusts in this study, suggesting that

149   the fluxes and mineralization related to wollastonite weathering in these two distinct natural

150   settings seem to be similar.

151   It is difficult to quantify mineralization rates, especially at Lewis, because ongoing work

152   at the site make it difficult to know the age of different cemented features. For example, the in-

153   situ cemented roadway sampled in 2018 (Fig. 1b) was buried by grading at the mine during the

154   next year; however, many of the berms did not appear to have been disturbed. Satellite imagery

155   does offer evidence that some of the stockpiles may have been in place at Lewis in 2006, but

156   satellite imagery does not offer similar insights for Fox Knoll. Although some of the cement

157   probably formed previous to each mine's respective closing, for consistency's sake,

158   mineralization rates were estimated using the end of the mining at each site (37 years prior to

159   sampling at Fox Knoll, and 2 years prior to sampling at Lewis). These calculations yield upper

160   limits of 0.09%/yr calcite and 0.02%/yr opal formation rates at Fox Knoll and 0.75%/yr calcite

161   and 0.22%/yr opal at Lewis. Note that these calculations are for cemented samples only and are

162   not representative of the unconsolidated material constituting the bulk of the two deposits. These

163   rates are comparable to preliminary results from a 19.5 month rooftop weathering experiment

164   using Lewis stockpile materials which yielded calcite production rates from pure wollastonite

165   ranging from 0.33–0.72%/yr for a fine sand fraction, and from 0.03–0.29%/yr in the medium-

166   coarse sand fraction (Kasten et al., 2022).

167   Textural evidence shows thin calcite and opal bands that coat wollastonite in samples

168   from both sites, often in multiple cycles of alternating layers (Fig. 2A), resembling those seen in

169   experiments (e.g. Daval et al., 2009b). However, preferential dissolution or secondary calcite +

170   silica formation on particular crystallographic faces (ie. Di Lorenzo et al., 2018) were not

171   observed. In lab experiments using aqueous solutions (Daval et al., 2009a; Di Lorenzo et al.,

172   2018), it was determined that dissolution is a rate-limiting step, and passivation of wollastonite

173   by reaction products (jacketing) can largely halt the reaction and carbonation. The level of

174   passivation in our field samples is hard to assess from textural observations, but it likely is not

175   strong here because discontinuous rims of calcite and opal are more commonly observed, and

176   fully-jacketed grains with little to no remaining wollastonite are also seen (Fig. 2C). This

177   suggests that a passivation control on wollastonite dissolution kinetics as seen in experiments is

178   not a feature of wollastonite weathering in the field.

179   Another feature seen in low-pH wollastonite dissolution experiments (e.g., Schott et al.,

180   2012) that was not observed in our field samples is the formation of leached layers due to

181   incongruent dissolution. Although dissolution features are evident in our samples (Figs. 2A–C),

182   they do not include the crazing or spallation that accompany leached-layer formation in

183   experiments at pH <4 (Schott et al., 2012), and leached zones are not seen in X-ray element

184   maps. Observed features are more consistent with congruent wollastonite dissolution, which

185   Schott et al. (2012) found to occur at pH >4. Soil pH measurements performed on berm pit

186   samples from Lewis, range from 7.0-8.0, supporting the presence of circumneutral conditions in

187   the stockpiles.

188

189   **Evidence from Isotopes**

190   Stable isotope and ^{14}C measurements of calcite from these sites are consistent with recent

191   cementation in the crushed ores and are not related to the orebody lithologies. Oxygen isotopes

192   are distinctly heavier than the low δ^{18}O values of silicates in these deposits (3.5 to -2.1‰; Valley

193   and O'Neil 1982; Barcello et al., 2018). Instead, oxygen isotope ratios more closely resemble

194   values found in soil carbonate in New York and elsewhere (e.g., Quade and Cerling 1993), and

195   are also consistent with calcite formation from local rainwater at ambient temperatures.

196   Calculations of calcite in equilibrium with monthly regional precipitation (Bowen, 2022) at a

197   range of average monthly temperatures (1981–2010 from ncei.noaa.gov, calculated using Kim

198   and O'Neil, 1997) yield δ^{18}O values that range from 17.0 to 25.3‰, which compares well with

199   the measured δ^{18}O(calcite) values of 15.3 to 23.8‰ for these sites.

200   Carbon isotope ratios at both mines are distinctly lighter from the minor lithologic

201   sources of C in mine rocks (Fig 3D). Rare calcite veins at Lewis have δ^{13}C= -3.1 to -2.7‰

202   (unpub. data), and marble from Lewis and Willsboro drill cores has δ^{13}C= -3.6 to -0.4‰ (Fig 3;

203   Valley and O'Neil 1982, and unpublished data for Lewis), which is typical for Adirondack

204   marbles (Kitchen and Valley, 1995).

205   The main differences in isotopic signatures at Lewis and Fox Knoll are related to their

206   carbon isotopes. At Lewis, δ^{13}C ratios are the lightest reported for calcite in the Adirondacks,

207   and they correlate with % calcite and % opal, with the most-cemented samples having the lowest

208    $\delta^{13}C$ (Fig 3C). These lowest $\delta^{13}C$ values also correspond with the highest fraction of modern C

209   ($F^{14}C$; Fig 3E), suggesting there is an older C source with $\delta^{13}C \approx$ -9‰ dominating the less

210   cemented samples, and a more recent source with $\delta^{13}C \approx$ -26‰ that is most prominent in well-

211   cemented samples. Fox Knoll samples have a more homogenous $\delta^{13}C \approx$ -7.5‰. These distinct

212    $\delta^{13}C$ signatures likely reflect differences in mineralization at the two mines.

213   The very low $\delta^{13}C$ of calcite at Lewis is notable. Values <-20‰ are rare in analogous

214   settings, such as soil carbonate, speleothems or secondary copper carbonates that typically accrue

215   low $\delta^{13}C$ from organic C (e.g., Quade and Cerling 1993; Melchiorre et al., 1999). The lack of

216   soil development and scant vegetation on stockpiles and within the pits (Fig. 1) suggest that soil

217   C is not abundant in mine samples. However, $\delta^{13}C$ values <-20‰ are commonly associated with

218   microbial activity and, along with the filamentous biofilms observed in cemented samples, point

219   to a potentially important microbial role in wollastonite dissolution and calcite formation at

220   Lewis (e.g., Xiao et al., 2015).

221   If these low $\delta^{13}C$ values are microbial in origin, the $\delta^{13}C$ of the two sites suggest that

222   microbes played an active role in weathering and calcite formation at Lewis but to a lesser extent

223   at Fox Knoll. This is plausible given the timing of mining at each site relative to the height of

224   acid precipitation and its well-documented toxic impacts on lake and forest ecosystems in the

225   Adirondacks. Microfauna studies have shown that low pH conditions and their associated S and

226   N compounds decrease microbial productivity (e.g., Baker et al., 1982; Shah et al., 2019). Other

227   studies have shown that SO_2 inhibits the activity of carbonic anhydrase (CA) (e.g., Rowlett et

228   al.,1991), a biotic enzyme that regulates carbonic acid production and carbonate mineralization

229   (e.g., Xiao et al., 2015).

230   The heyday of mining at Fox Knoll spanned the peak of strong acid precipitation, which

231   could have suppressed both microbial productivity and the activity of microbial CA. If so, at

232   least some wollastonite weathering at Fox Knoll perhaps would have occurred abiotically under

233   acidic conditions, resulting in higher $\delta^{13}C$ values. Conversely, most mining at Lewis took place

234   after Clean Air legislation was in place, potentially allowing microbial populations and their role

235   in wollastonite dissolution and carbonation to rebuild. Such a recovery is supported by Lui et al.

236   (2020), who saw a recovery of microbial populations over time after simulated acid rain

237   treatments were stopped. Microbial communities and their associated CA have been seen to

238   enhance wollastonite dissolution (Xiao, 2015). CA accelerates CO_2 hydration rates, and when

239   calcium is present in solutions with pH $\geq$ 7 (as seen here), it readily combines with hydrated CO_2

240   to precipitate as $CaCO_3$ (Kim et al., 2012).

241   An alternate interpretation of very low $\delta^{13}C$ is important to evaluate. Similar values have

242   been reported in carbonate minerals from highly alkaline waters, especially in anthropogenic

243   settings such as weathering concrete, slag, and incinerator ash (see Fléhoc et al., 2006). Water in

244   equilibrium with wollastonite at ambient conditions has pH =10.7 (Huijgen et al., 2006), so pore

245   water in crushed wollastonite ore could potentially be quite alkaline. However, calcite formed

246   from highly alkaline waters is characterized by strongly correlated $\delta^{13}C$ and $\delta^{18}O$ depletions

247   (R^2>0.9 in many studies; Fig. 4A) caused primarily by kinetic isotope effects related to

248   hydroxylation reactions (Dietzel et al., 1992). Although some overlap in isotope ratios occurs

249   between some of these studies and our data, our $\delta^{13}C$ and $\delta^{18}O$ values are not correlated and

250   therefore, are likely not caused by these kinetic effects.

251   Carbonate precipitation from moderately alkaline waters (pH= 8 to 11) has also been

252   observed to result in low $\delta^{13}C$ values for carbonate minerals, while oxygen isotope ratios show

253   equilibrium with the supernatant under these conditions (e.g. O'Neil and Barnes, 1971). In these

254   settings, carbon isotope fractionation is attributed to kinetic effects related to atmospheric CO_2

255   diffusion into solution (Dietzel et al., 1992; Wilson et al., 2010). Although this isotope effect

256   could explain some of the carbon isotope depletions we observe at our field sites, there are

257   important differences. Field examples of this style of carbonation yield $\delta^{13}C$ values of

258   carbonates (typically > -15‰; O'Neil and Barnes, 1971; Dietzel et al., 1992) that are not as low

259   as those we observe at Lewis. Additionally, experiments showing these isotope effects at a

260   moderately alkaline pH yield a negative trend between $\delta^{13}C$ and $\delta^{18}O$ for carbonate (in this case

261   dypingite formation; Wilson et al., 2010), a relationship which is not observed in our data.

262   Finally, if this were the mechanism controlling the carbon isotope fractionation at our sites, it is

263   unclear why Fox Knoll calcite (with less negative and more constrained $\delta^{13}C$ values of -6 to -

264   12‰) would show such different kinetic isotope effects from Lewis calcite (with $\delta^{13}C$ values

265   ranging from -9 to -30‰), considering both mines are proximately located and contain nearly

266   identical wollastonite ore.

267   Several case studies of weathering and C capture over the past decade have examined

268   deposits in ultramafic rocks (Fig. 4B). Secondary carbonates in most of these studies have high

269    $\delta^{13}C$ and $\delta^{18}O$ in equilibrium with surface waters and atmospheric CO_2, sometimes kinetically

270   modified or mixed with lithologic O and C. However, one ultramafic deposit, the Diavik

271   diamond mine, does show very low $\delta^{13}C$ in secondary carbonates associated with sewage water

272   disposal ($\delta^{13}C$= -26.3 to -13.0‰; Wilson et al., 2011). The authors note that this ^{13}C depletion

273   may be caused by 1) an organic source of the carbon (ie., the sewage) or 2) kinetic effects in a

274   pH>11 solution, as further supported by a correlation between $\delta^{13}C$ and $\delta^{18}O$ there (e.g., compare

275   Figs. 4A and 4B). Although the very low $\delta^{13}C$ in Diavik samples may point to possible

276   microbial C isotope fractionation, similar to what we are proposing for Lewis, carbon isotope

277   ratios this low are not observed at other studied (see Fig 4B) ultramafic-hosted deposits.

278

279   **Implications**

280   The magnitude of anthropogenic CO_2 emissions and its impact on climate suggests that a

281   variety of sequestration strategies are likely to be used over coming decades (Oelkers and Cole,

282   2008). Carbonation of mine wastes as a strategy for CO_2 capture mainly has been studied in

283   ultramafic lithologies. Power et al. (2013) estimate that with engineered C capture, mine wastes

284   have the potential to sequester ca. 600 Mt CO_2/yr worldwide, a possibility that is largely

285   unrealized. Based on this 'accidental' C capture experiment, our wollastonite mine data may

286   inform engineering approaches to carbonation of a variety of rock types.

287   Weathering under the climatic conditions of northeastern North America causes extensive

288   wollastonite dissolution, and stable isotopes can be used to fingerprint C capture. Textural

289   association of calcite with wollastonite, modern $F^{14}C$ values, and calcite's rarity in deposit rocks

290   allows the $\delta^{13}C$ of sequestered C to be assessed directly at Lewis and Fox Knoll. Carbon isotopes

291   point towards the importance of microbial C isotope fractionation at Lewis. Our findings of the

292   very low $\delta^{13}C$ associated with biofilms and other organic features in these ore stockpiles help to

293   support the potential for biologically enhancing C sequestration during silicate weathering, and

294   the potential role of acid precipitation in influencing sequestration pathways.

295

296   **Acknowledgments**

306   **References cited**

307   Baker, M.D., Inniss, W.E., Mayfield, C.I., and Wong, P.T.S. (1982) Effect of pH on the growth

308   and activity of heterotrophic sediment microorganisms. Chemosphere, 11, 973–983.

309

310   Barcello, J.C., Daggett, L.H., Peck, W.H., and Valley, J.W. (2018) Low oxygen isotope ratios in

311   garnet from the Lewis deposit, Adirondack Highlands. Geological Society of America Abstracts

312   with Programs, 50(2), 10.1130/abs/2018NE-311021.

313

314   Bowen, G.J. (2017) The Online Isotopes in Precipitation Calculator, version 3.1.

315   http://www.waterisotopes.org.

316

317   Cerling, T.E., and Quade, J. (1993) Stable carbon and oxygen Isotopes in soil carbonates. In P.K.

318   Swart, K.C. Lohmann, K. McKenzie, and S. Savin, Eds., Climate Change in Continental Isotopic

319   Records, American Geophysical Union Geophysical Monograph Series Vol. 78, pp. 217–231.

320

321   Daval, D., Martinez, I., Corvisier, J., Findling, N., Goffé, B., and Guyot, F. (2009a) Carbonation

322   of Ca-bearing silicates, the case of wollastonite: Experimental investigations and kinetic

323   modeling. Chemical Geology, 265, 63–78.

324

325   Daval, D., Martinez, I., Guigner, J.-M., Hellmann, R., Corvisier, J., Findling, N., Dominici, C.,

326   Goffe, B., and Guyot, F. (2009b) Mechanism of wollastonite carbonation deduced from micro- to

327   nanometer length scale observations. American Mineralogist, 94, 1707–1726.

328

329   Di Lorenzo, F., Ruiz-Agudo, C., Ibañez-Velasco, A., Gil-San Millán, R., Navarro, J., Ruiz-

330   Agudo, E., and Rodriguez-Navarro, C. (2018) The carbonation of wollastonite: A model reaction

331   to test natural and biomimetic catalysts for enhanced CO_2 sequestration. Minerals, 8, 209.

332

333   Eberl, D.D. (2003) User's Guide to RockJock – A Program for Determining Quantitative

334   Mineralogy from Powder X-Ray Diffraction Data, US Geological Survey Open-File Report

335   2003–78., 47 p.

336

337   Fléhoc, C., Girard, J.-P., Piantone, P., and Bodénan, F. (2006) Stable isotope evidence for the

338   atmospheric origin of CO_2 involved in carbonation of MSWI bottom ash. Applied Geochemistry,

339   21, 2037–2048.

340

341   Gras, A., Beaudoin, G., Molson, J., and Plante, B. (2020) Atmospheric carbon sequestration in

342   ultramafic mining residues and impacts on leachate water chemistry at the Dumont Nickel

343   Project, Quebec, Canada. Chemical Geology, 546, 119661.

344

345   Haque, F., Santos, R.M., and Chiang, Y.W. (2020) CO_2 sequestration by wollastonite-amended

346   agricultural soils – An Ontario field study. International Journal of Greenhouse Gas Control, 97,

347   103017.

348

349   Huijgen, W.J.J., Witkamp, G.-J., and Comans, R.N.J. (2006) Mechanisms of aqueous

350   wollastonite carbonation as a possible CO_2 sequestration process. Chemical Engineering Science,

351   61, 4242–4251.

352

353   Kasten, S., Inoa, M., Keller, D., and Peck, W. (2022) Weathering and carbon sequestration at

354   New York wollastonite mines. Geological Society of America Abstracts with Programs, 54(3),

355   10.1130/abs/2022NE-374686.

356

357   Kim, S.-T., and O'Neil, J.R. (1997) Equilibrium and nonequilibrium oxygen isotope effects in

358   synthetic carbonates. Geochimica et Cosmochimica Acta, 61, 3461–3475.

359

360   Kitchen, N.E., and Valley, J.W. (1995) Carbon isotope thermometry in marbles of the

361   Adirondack Mountains, New York. Journal of Metamorphic Geology, 13, 577–594.

362

363   Lackner, K.S., Park, A.-H.A., and Zhao, H. (2012) Disposing of Greenhouse Gases through

364   Mineralization Using the Wollastonite Deposits of New York State, New York State Energy

365   Research and Development Authority Final Report 12–14., 28 p.

366

367   Likens, G.E., Butler, T.J., Claybrooke, R., Vermeylen, F., and Larson, R. (2021) Long-term

368   monitoring of precipitation chemistry in the U.S.: Insights into changes and condition.

369   Atmospheric Environment, 245, 118031.

370

371   Melchiorre, E.B., Criss, R.E., and Rose, T.P. (2000) Oxygen and carbon isotope study of natural

372   and synthetic azurite. Economic Geology, 95, 621–628.

373

374   Milodowski, A.E., Rochelle, C.A., Lacinska, A., and Wagner, D. (2011) A natural analogue

375   study of CO_2-cement interaction: Carbonation of calcium silicate hydrate-bearing rocks from

376   Northern Ireland. Energy Procedia, 4, 5235–5242.

377

378   Oelkers, E.H., and Cole, D.R. (2008) Carbon dioxide sequestration a solution to a global

379   problem. Elements, 4, 305–310.

380

381   O'Neil, J.R., and Barnes, I. (1971). C^{13} and O^{18} compositions in some fresh-water carbonates

382   associated with ultramafic rocks and serpentinites: Western United States. Geochimica et

383   Cosmochimica Acta, 35, 687–697.

384

385   Oskierski, H.C., Dlugogorski, B.Z., and Jacobsen, G. (2013) Sequestration of atmospheric CO_2

386   in chrysotile mine tailings of the Woodsreef Asbestos Mine, Australia: Quantitative mineralogy,

387   isotopic fingerprinting and carbonation rates. Chemical Geology, 358, 156–169.

388

389   Peck, W.H., and Bailey, E. (2008) Origin of the Lewis wollastonite deposit. In B.W. Selleck,

390   Ed., Field Trip Guidebook for 80th annual meeting of the New York State Geological

391   Association, Lake George, New York, Colgate University pp. 130–135.

392

393   Peck, W.H., DeAngelis, M.T., Meredith, M.T., and Morin, E. (2005) Polymetamorphism of

394   marbles in the Morin terrane, Grenville Province, Quebec. Canadian Journal of Earth Sciences,

395   42, 1949–1965.

396

397   Peck, W.H., Selleck, B.W., Regan, S.P., Howard, G.E., and Kozel, O.O. (2018) In-situ dating of

398   metamorphism in Adirondack anorthosite. American Mineralogist, 103, 1523–1529.

399

400   Power, I.M., Harrison, A.L., Dipple, G.M., Wilson, S.A., Kelemen, P.B., Hitch, M., and

401   Southam, G. (2013) Carbon mineralization: From natural analogues to engineered systems.

402   Reviews in Mineralogy and Geochemistry, 77, 305–360.

403

404   Robinson, S., Santini, K., and Moroney, J. (2006) Wollastonite. In J.E. Kogel, N.C. Trivedi, J.M.

405   Barker, and S.T. Krukowski, Eds., Industrial Minerals & Rocks: Commodities, Markets, and

406   Uses, Society for Mining, Metallurgy, and Exploration pp. 1027–1037. Littleton, Colo.

407

408   Rowlett, R.S., Gargiulo, N.J., Santoli, F.A., Jackson, J.M., and Corbett, A.H. (1991) Activation

409   and inhibition of bovine carbonic anhydrase III by dianions. Journal of Biological Chemistry,

410   266, 933–941.

411

412   Schott, J., Pokrovsky, O.S., Spalla, O., Devreux, F., Gloter, A., and Mielczarski, J.A. (2012)

413   Formation, growth and transformation of leached layers during silicate minerals dissolution: The

414   example of wollastonite. Geochimica et Cosmochimica Acta, 98, 259–281.

415

416   Seman, S., Stockli, D.F., and McLean, N.M. (2017) U-Pb geochronology of grossular-andradite

417   garnet. Chemical Geology, 460, 106–116.

418

419   Shah, T., Shah, Z., Shah, S.A.A., and Ahmad, N. (1970) Nitrogen mineralization and microbial

420   activity as influenced by sulfur sources in an alkaline calcareous soil. Journal of Scientific

421   Agriculture, 14–18.

422

423   Shao, S., Driscoll, C.T., Johnson, C.E., Fahey, T.J., Battles, J.J., and Blum, J.D. (2016) Long-

424   term responses in soil solution and stream-water chemistry at Hubbard Brook after experimental

425   addition of wollastonite. Environmental Chemistry, 13, 528.

426

427   Urey, H. C. (1952) The Planets: Their Origin and Development. Yale Univ. Press, New Haven,

428   Conn.

429

430   Valley, J.W., and O'Neil, J.R. (1982) Oxygen isotope evidence for shallow emplacement of

431   Adirondack anorthosite. Nature, 300, 497–500.

432

433   Whitney, P.R., and Olmsted, J.F. (1998) Rare earth element metasomatism in hydrothermal

434   systems: the Willsboro-Lewis wollastonite ores, New York, USA. Geochimica et Cosmochimica

435   Acta, 62, 2965–2977.

436

437   Wilson, S.A., Barker, S.L., Dipple, G.M., and Atudorei, V. (2010). Isotopic disequilibrium

438   during uptake of atmospheric CO_2 into mine process waters: Implications for CO_2 sequestration.

439   Environmental Science & Technology, 44, 9522-9529.

440

441   Wilson, S.A., Dipple, G.M., Power, I.M., Thom, J.M., Anderson, R.G., Raudsepp, M., Gabites,

442   J.E., and Southam, G. (2009) Carbon dioxide fixation within mine wastes of ultramafic-hosted

443   ore feposits: Examples from the Clinton Creek and Cassiar chrysotile deposits, Canada.

444   Economic Geology, 104, 95–112.

445

446   Wilson, S.A., Dipple, G.M., Power, I.M., Barker, S.L.L., Fallon, S.J., and Southam, G. (2011)

447   Subarctic Weathering of Mineral Wastes Provides a Sink for Atmospheric CO_2. Environmental

448   Science & Technology, 45, 7727–7736.

449

450   Wilson, S.A., Harrison, A.L., Dipple, G.M., Power, I.M., Barker, S.L.L., Ulrich Mayer, K.,

451   Fallon, S.J., Raudsepp, M., and Southam, G. (2014) Offsetting of CO_2 emissions by air capture

452   in mine tailings at the Mount Keith Nickel Mine, Western Australia: Rates, controls and

453   prospects for carbon neutral mining. International Journal of Greenhouse Gas Control, 25, 121–

454   140.

455

456   Xiao, L., Lian, B., Hao, J., Liu, C., and Wang, S. (2015) Effect of carbonic anhydrase on silicate

457   weathering and carbonate formation at present day CO_2 concentrations compared to primordial

458   values. Scientific Reports, 5, 7733.

459

460   **Figure captions**

461   Figure 1. Field photos of cemented crushed wollastonite ore, showing % calcite, $\delta^{13}C$ (VPDB),

462   and % modern carbon ($F^{14}C$). (A) Cemented hardpan at Lewis. (B) Berm cap crust at Lewis. (C)

463   Berm cap crust at Fox Knoll. Scale bar = 10 cm. (D) Cemented boulder in Fox Knoll open pit.

464   Note the scant vegetation in all photos.

465

466   Figure 2. Representative textures in cemented wollastonite ores. (A) Backscattered electron

467   (BSE) image of calcite (C) & opal (S) rinds on wollastonite (W). (B) BSE image of cleavage and

468   pore-filling calcite and opal cements. (C) BSE image of opal & calcite stockworks on highly

469   dissolved wollastonite. (D & E) Secondary electron (SE) images of ridged calcite & opal

470   lepidospheres & coatings, (E) also shows the platy mineral. (F) SE image of biofilms and organic

471   filaments.

472

473   Figure 3. Mineralogy, stable isotope ratios, and ^{14}C of crushed ore samples from the Lewis and

474   Fox Knoll mines. Arrows show the stoichiometry of reaction (1).

475

476   Figure 4. Stable isotopes of calcite cements in crushed wollastonite ores compared to other

477   secondary carbonates and carbonate reservoirs (A) Adirondack marbles and isotope effects

478   commonly observed in secondary and anthropogenic calcites (after Kitchen and Valley, 1995;

479   Melchiorre et al., 1999; Fléhoc et al., 2006). (B) Secondary carbonates at select ultramafic-

480   hosted mineral deposits (Wilson et al., 2009; 2011; 2014; Oskierski et al., 2013; Gras et al.,

481   2017).

482

483

Table 1. Mineralogy and stable isotopes of cemented wollastonite from the Lewis and Fox Knoll wollastonite mines.

Sample	Calcite %	Opal %	Wollastonite %	Garnet %	Pyroxene %	Quartz %	Plagioclase %	Kspar %	$\delta^{18}O$ (VSMOW)	$\delta^{13}C$ (VPDB)	$F(^{14}C)$
Cemented samples from the Lewis Mine. Lat 44.3031, Long -73.6139, WGS84											
PB18 1 C	0.83	0.16	9.03	82.36	6.21	0.25	0.38	0.78	15.51	-20.25	
PB18 2 C	1.67	0.50	20.63	74.47	2.50	0.02	0.00	0.19	15.34	-25.33	
PB18 3 C	1.58	0.56	17.72	67.84	6.48	1.69	0.57	3.56	21.91	-19.30	
PB18 4 C	2.82	0.65	19.68	62.87	8.08	1.28	0.44	4.18	20.84	-25.54	1.0381 +/- 0.0039
PB18 5 C	0.67	0.26	7.10	80.46	11.02	0.24	0.00	0.24	17.59	-21.44	
18LEW1 C	1.47	0.56	7.14	79.58	10.98	0.01	0.00	0.26	17.87	-28.50	1.0252 +/- 0.0038
Lewis Mine ore stockpile berm transect. Lat 44.3030, Long -73.6143, WGS84											
LBP18 0-5	0.39	0.23	42.00	46.92	7.86	0.00	2.30	0.30	15.54	-11.85	0.7445 +/- 0.0028
LBP18 5-10	0.36	0.10	33.44	62.11	3.57	0.00	0.29	0.12	18.37	-9.25	
LBP18 10-15	0.19	0.19	50.66	45.76	3.02	0.00	0.16	0.00	17.41	-13.05	
LBP18 15-20	0.14	0.04	42.45	54.64	2.15	0.00	0.27	0.30			
LBP18 25-30	0.04	0.10	34.44	60.90	3.75	0.26	0.19	0.31			
LBP18 35-40	0.09	0.06	28.76	66.60	3.92	0.12	0.02	0.41	16.64	-10.45	
LBP18 45-50									17.28	-17.34	
LBP18 85-90	1.17	0.29	17.75	76.41	4.33	0.02	0.03	0.02			
LBP18 100-105	0.82	0.33	46.20	50.17	2.15	0.00	0.18	0.14	19.31	-13.31	
Lewis Mine roadside berm transect. Lat 44.3025, Long -73.6142, WGS84											
CB18 Hat C	0.69	0.28	18.05	74.35	5.43	0.30	0.43	0.45	18.15	-16.68	0.8907 +/- 0.0033
CB18 0-5 C	0.80	0.24	17.44	73.01	7.07	0.32	0.87	0.24	22.97	-16.82	
CB18 0-5	0.77	0.09	14.34	78.27	5.60	0.27	0.45	0.23			
CB18 5-10	0.43	0.16	20.30	70.83	7.93	0.12	0.08	0.15			
CB18 10-15	0.64	0.28	15.83	75.58	6.09	0.20	0.92	0.46	21.36	-14.62	
CB18 15-20	0.64	0.05	25.10	66.96	6.64	0.24	0.07	0.30			
Lewis Mine fine-grained splits											
PB18 1 Cf	2.04	0.63	15.55	74.33	4.46	0.92	1.30	0.76	18.89	-19.26	
PB18 2 Cf	2.28	0.68	30.95	62.93	2.30	0.14	0.54	0.19	18.58	-24.87	
LBP18 35-42 Cf	1.85	0.39	23.31	69.51	3.40	0.27	0.84	0.44			
CB18 Hat Cf	1.17	0.35	23.64	70.36	2.49	0.47	0.95	0.57			
CB18 0-5 Cf	1.52	0.42	19.84	70.56	5.80	0.39	1.15	0.34	20.70	-17.48	
CB18 10-15 f	0.75	0.22	13.37	78.44	5.19	0.38	1.00	0.63	19.09	-12.31	
Fox Knoll Mine cemented agglomerates, Lat 44.3486, Long -73.4342, WGS84											
FK 19-1 C	2.92	0.43	39.98	53.98	2.09	0.21	0.00	0.40	20.40	-8.55	
FK 19-3 C	2.94	0.60	45.72	47.87	2.43	0.06	0.37	0.00	20.71	-6.97	
FK 19-4 C	6.09	1.66	33.61	55.12	3.12	0.39	0.11	0.00	20.56	-7.88	0.9645 +/- 0.0036
FK 19-16 C	4.30	1.24	32.72	57.17	4.23	0.30	0.03	0.00	21.42	-7.08	
Fox Knoll Mine berm transect. Lat 44.3484, Long -73.4337, WGS84											
FK 19-5 0-5 C	1.8	0.25	41.24	52.05	3.8	0.39	0.04	0.43	20.23	-6.60	
FK 19-6 15-20 C	2.19	0.29	42.18	48.37	2.66	2.49	1.27	0.54	19.25	-7.10	0.6639 +/- 0.0025
FK 19-7 35-40									20.80	-7.29	
FK 19-8 55-60	1.92	0.11	34.05	53.19	3.68	4.07	2.36	0.62	22.01	-6.29	
FK 19-9 75-80	1.70	0.26	22.82	67.29	2.55	2.02	0.63	2.71	19.95	-7.42	
FK 19-10 85-90									19.44	-8.72	
FK 19-11 95-100									19.89	-7.42	
FK 19-12 105-110	1.64	0.39	24.7	68.57	1.77	1.18	1.13	0.62	23.78	-7.56	
FK 19-13 115-120									18.42	-11.67	
FK 19-15 135-140	1.64	0.26	43.19	50.98	3.13	0.63	0.09	0.09			

Notes: C denotes cemented samples. Samples with f are fine-grained splits. Numbers (e.g. 5-10) are depth in transects (in cm).
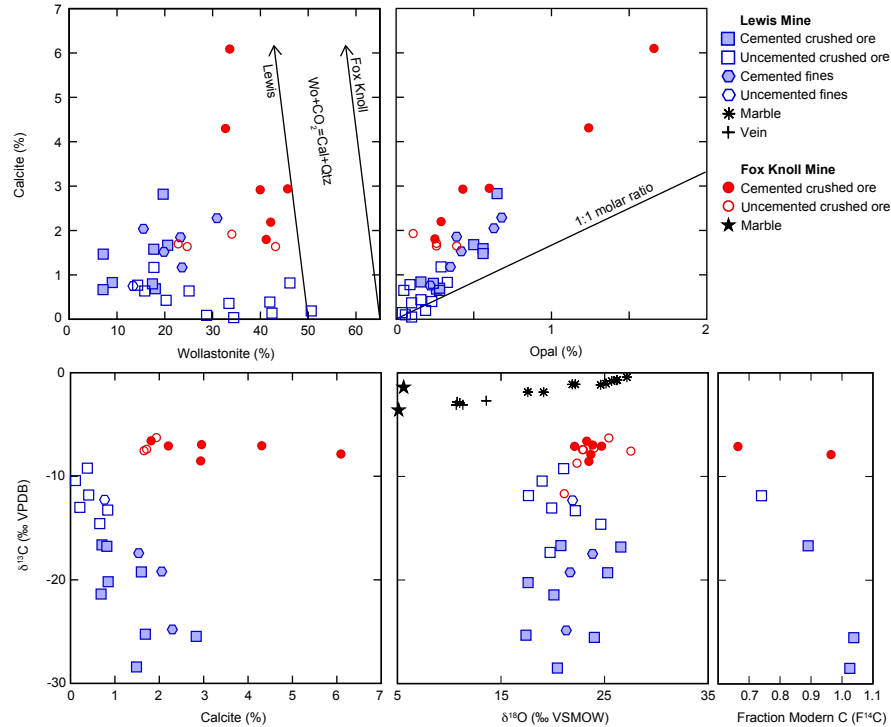
Peck et al. Figure 1
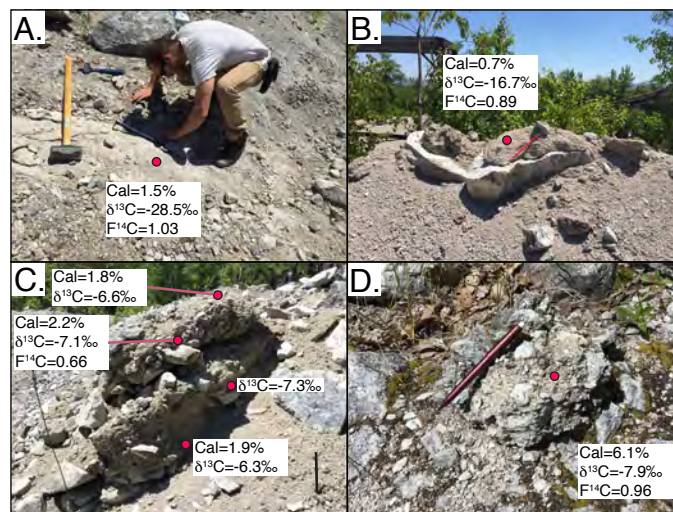
Peck et al. Figure 2
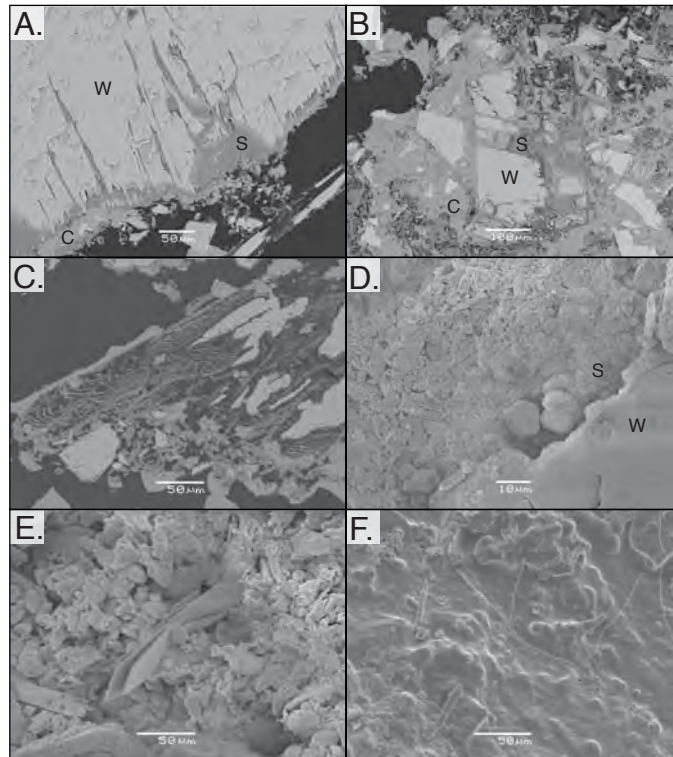
Peck et al. Figure 3

Peck et al. Figure 4